

How do External Companions Affect Spin-Orbit Misalignment of Hot Jupiters?

Dong Lai^{*}, Kassandra R. Anderson and Bonan Pu

Cornell Center for Astrophysics and Planetary Science, Department of Astronomy, Cornell University, Ithaca, NY 14853, USA

1 November 2017

ABSTRACT

Consider a planet with its orbital angular momentum axis aligned with the spin axis of its host star. To what extent does an inclined distant companion (giant planet or binary star) affect this alignment? We provide an analytic, quantitative answer and apply it to hot Jupiter systems, for which misalignments between the orbital axis and the stellar spin axis have been detected. We also show how similar consideration can be applied to multi-planet systems with distant companions (such as Kepler-56). The result of this paper provides a simple method to assess the dynamical role played by external companions on spin-orbit misalignments in exoplanetary systems.

Key words: planetary systems — planets and satellites: dynamical evolution and stability — planets and satellites: formation — stars: individual (HAT-P-13, WASP-41, WASP-47, WASP-22, Kepler-56)

1 INTRODUCTION

Many hot Jupiters (HJs, giant planets with orbital periods about 5 days or less) are known to have a misaligned orbital angular momentum axis with respect to the spin axis of their host stars (e.g. Winn & Fabrycky 2015). The origin of this spin-orbit misalignment and the formation mechanisms of HJs remain under debate. The possibilities include high-eccentricity migration induced by additional giant planets or stellar companions (e.g., Fabrycky & Tremaine 2007; Wu et al. 2007; Nagasawa et al. 2008; Wu & Lithwick 2011; Naoz et al. 2012; Beauge & Nesvornyy 2012; Storch et al. 2014; Petrovich 2015; Anderson et al. 2016; Muñoz et al. 2016) and migration in protoplanetary disks that are misaligned with the host stars (e.g. Bate et al. 2010; Lai et al. 2011; Batygin 2012; Batygin & Adams 2013; Lai 2014; Spalding & Batygin 2014).

A large fraction ($\sim 70\%$) of HJ systems have been found to have external companions, either gas giants at large semi-major axes (1-20 au) (Knutson et al. 2014; Bryan et al. 2016) or distant (50-2000 au) stellar companions (Ngo et al. 2015; Wang et al. 2015). How these companions might have facilitated the formation of misaligned HJs is an important question, but often may not have an unambiguous answer (e.g. Ngo et al. 2016; Atonini et al. 2016). A simpler question to ask is how an observed companion may affect the current state of spin-orbit misalignment. The answer to this question, when combined with observational data, may help

constrain the property of the companion. The purpose of this paper is to provide such an answer in quantitative way (Section 2), to allow quick assessment/constraint of the dynamical role of external companions on spin-orbit misalignments, without formal celestial mechanics calculations (e.g. Boué & Fabrycky 2014) or N-body integrations with large parameter space. In Section 3, we illustrate our result by applying it to several HJ systems with external companions. A recent work (Becker et al. 2017) did not include the gravitational coupling between the HJ and the oblate host star; this coupling can in fact play an important role in determining how spin-orbit misalignments are affected by the companion.

Spin-orbit misalignment has been detected in at least one multi-planet system (Kepler-56; Huber et al. 2013). Our analysis can be generalized to such systems. This is discussed in Section 4 using Kepler-56 as an example.

2 EQUATIONS AND ANALYTICAL RESULTS

Consider a planet of mass m_1 on a circular orbit (with semi-major axis a_1) around a central star (mass M_* and spin angular momentum vector \mathbf{S}_*). The orbital angular momentum vector of the planet is \mathbf{L}_1 . An external perturber (mass m_p) moves on an inclined orbit, with semi-major axis a_p , eccentricity e_p and inclination θ_p (the angle between \mathbf{L}_1 and \mathbf{L}_p , the orbital angular momentum of the perturber). How is the spin-orbit misalignment angle θ_{*1} (the angle between \mathbf{S}_* and \mathbf{L}_1 influenced by the perturber?

* Email: dong@astro.cornell.edu

We denote the relevant (spin and orbital) angular momentum vectors by $\mathbf{S}_* = S_* \hat{\mathbf{s}}_*$, $\mathbf{L}_1 = L_1 \hat{\mathbf{l}}_1$ and $\mathbf{L}_p = L_p \hat{\mathbf{l}}_p$, where $\hat{\mathbf{s}}_*$, $\hat{\mathbf{l}}_1$ and $\hat{\mathbf{l}}_p$ are unit vectors. The evolution equations for $\hat{\mathbf{s}}_*$, $\hat{\mathbf{l}}_1$ and $\hat{\mathbf{l}}_p$ are

$$\frac{d\hat{\mathbf{s}}_*}{dt} = \omega_{*1}(\hat{\mathbf{l}}_1 \cdot \hat{\mathbf{s}}_*)(\hat{\mathbf{s}}_* \times \hat{\mathbf{l}}_1) + \omega_{*p}(\hat{\mathbf{s}}_* \cdot \hat{\mathbf{l}}_p)(\hat{\mathbf{s}}_* \times \hat{\mathbf{l}}_p), \quad (1)$$

$$\frac{d\hat{\mathbf{l}}_1}{dt} = \omega_{1*}(\hat{\mathbf{l}}_1 \cdot \hat{\mathbf{s}}_*)(\hat{\mathbf{l}}_1 \times \hat{\mathbf{s}}_*) + \omega_{1p}(\hat{\mathbf{l}}_1 \cdot \hat{\mathbf{l}}_p)(\hat{\mathbf{l}}_1 \times \hat{\mathbf{l}}_p), \quad (2)$$

$$\frac{d\hat{\mathbf{l}}_p}{dt} = \omega_{p*}(\hat{\mathbf{l}}_p \cdot \hat{\mathbf{s}}_*)(\hat{\mathbf{l}}_p \times \hat{\mathbf{s}}_*) + \omega_{p1}(\hat{\mathbf{l}}_p \cdot \hat{\mathbf{l}}_1)(\hat{\mathbf{l}}_p \times \hat{\mathbf{l}}_1). \quad (3)$$

Each term in the above equations has a clear physical meaning. The characteristic precession rate of $\hat{\mathbf{s}}_*$ around $\hat{\mathbf{l}}_1$ (driven by m_1) is given by

$$\omega_{*1} = \frac{3k_{q*}}{2k_*} \left(\frac{m_1}{M_*} \right) \left(\frac{R_*}{a_1} \right)^3 \Omega_*, \quad (4)$$

where $\Omega_* = 2\pi/P_*$ is the angular frequency of the host star, and k_* , k_{q*} are defined through the star's moment of inertia and quadrupole moment: $I_3 = k_* M_* R_*^2$ and $I_3 - I_1 = k_{q*} \hat{\Omega}_*^2 M_* R_*^2$, with $\hat{\Omega}_* = \Omega_* (GM_*/R_*^3)^{-1/2}$. Typical values (for solar type stars) are $k_* \simeq 0.06$ and $k_{q*} \simeq 0.01$ (Mecheri et al. 2004; Lai 2016). Similarly, the characteristic precession rate of $\hat{\mathbf{s}}_*$ around $\hat{\mathbf{l}}_p$ (driven by m_p) is given by

$$\omega_{*p} = \frac{3k_{q*}}{2k_*} \left(\frac{m_p}{M_*} \right) \left(\frac{R_*}{\tilde{a}_p} \right)^3 \Omega_*, \quad (5)$$

where we have defined the ‘‘effective’’ semi-major axis $\tilde{a}_p \equiv a_p \sqrt{1 - e_p^2}$. The characteristic precession rate of $\hat{\mathbf{l}}_1$ around $\hat{\mathbf{s}}_*$ (driven by the stellar quadrupole) is given by

$$\omega_{1*} = \omega_{*1} \left(\frac{S_*}{L_1} \right). \quad (6)$$

The characteristic precession rate of $\hat{\mathbf{l}}_1$ around $\hat{\mathbf{l}}_p$ (driven by m_p) is given by

$$\omega_{1p} = \frac{3m_p}{4M_*} \left(\frac{a_1}{\tilde{a}_p} \right)^3 n_1, \quad (7)$$

where n_1 is the mean motion of m_1 . The two precession frequencies characterizing the evolution of $\hat{\mathbf{l}}_p$ are

$$\omega_{p*} = \omega_{*p} \left(\frac{S_*}{L_p} \right), \quad \omega_{p1} = \omega_{1p} \left(\frac{L_1}{L_p} \right). \quad (8)$$

Obviously, when $L_p \gg L_1$ and $L_p \gg S_*$, we can consider $\hat{\mathbf{l}}_p$ fixed in time.

The above assumes a circular orbit for m_1 . An inclined perturber may also excite eccentricity. But this is suppressed by various short-range forces for close-in planets (e.g. Liu et al. 2015): For example, the pericenter precession rate due to General Relativity, $(3GM_*/c^2 a_1) n_1$, is much larger than the Lidov-Kozai rate, $(m_p/M_*)(a_1/\tilde{a}_p)^3 n_1$, for systems of interest in this paper.

2.1 Results

Given initial conditions, equations (1)-(3) can be easily integrated to determine the time evolution of θ_{*1} and its maximum value. Figure 1 shows some examples of $(\theta_{*1})_{\max}$ for initially spin-orbit aligned systems ($\theta_{*1} = 0$, but $\theta_p \neq 0$) with various parameters.

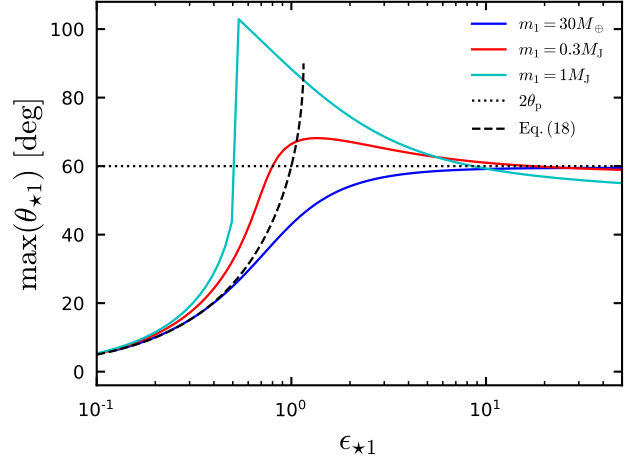


Figure 1. Maximum misalignment angle between $\hat{\mathbf{l}}_1$ and $\hat{\mathbf{s}}_*$ in the presence of an external inclined perturber (m_p). Initially $\hat{\mathbf{l}}_1$ and $\hat{\mathbf{s}}_*$ are aligned, and both inclined relative to $\hat{\mathbf{l}}_p$ at $\theta_p = 30^\circ$. We fix the HJ and stellar parameters to those of WASP-41 (see Section 3), but allow m_1 to take various values. Different solid lines correspond to different values of m_1 ($= 30M_\oplus, 0.3M_J, 1M_J$, corresponding to $L_1/S_* = 0.9, 2.9, 9.7$). The dimensionless coupling parameter ϵ_{*1} (Eq. 9) is varied by varying the ‘‘strength’’ of the perturber, m_p/\tilde{a}_p^3 . Analytical results in the strong (planet-star) coupling and weak coupling limits are also shown. A resonance feature is present around $\epsilon_{*1} \sim 1$ when $L_1/S_* \gtrsim 1$. Note that in general $(\theta_{*1})_{\max}$ depends on various physical parameters through ϵ_{*1} , L_1/S_* and θ_p (and L_p/L_1 when it is not much larger than unity).

The problem we consider here is analogous to the problem of the evolution of the mutual inclination of two planets under the influence of an inclined, distant perturber (Lai & Pu 2017). A key dimensionless parameter is

$$\epsilon_{*1} \equiv \frac{\omega_{1p} - \omega_{*p}}{\omega_{*1} + \omega_{1*}}, \quad (9)$$

which measures the strength of planet-star coupling relative to the ‘‘disruptive’’ forcing of the perturber (planet-star coupling increases with decreasing ϵ_{*1}). While there are many physical parameters in this problem (m_1 , m_p , a_1 , a_p , stellar spin, etc), the shape of the $(\theta_{*1})_{\max} - \epsilon_{*1}$ curve shown in Fig. 1 (for initial aligned systems) depends only on L_1/S_* and θ_p (and somewhat on L_p/L_1 when L_p is only moderately larger than L_1).

There are three regimes for the behaviors of θ_{*1} evolution:

(i) *Weak (planet-star) coupling regime* ($\epsilon_{*1} \gg 1$). In this regime, both $\hat{\mathbf{l}}_1$ and $\hat{\mathbf{l}}_p$ precess around $\mathbf{J} = \mathbf{L}_1 + \mathbf{L}_p = J\hat{\mathbf{J}}$ at a rapid rate:

$$\frac{d\hat{\mathbf{l}}_{1,p}}{dt} \simeq \left(\frac{J\omega_{1p}}{L_p} \cos \theta_p \right) \hat{\mathbf{l}}_{1,p} \times \hat{\mathbf{J}}, \quad (10)$$

with a constant θ_{1J} (the angle between $\hat{\mathbf{l}}_1$ and \mathbf{J}) given by $\sin \theta_{1J} = (L_p/J) \sin \theta_p$, where $J = |\mathbf{J}| = (L_1^2 + L_p^2 + 2L_1L_p \cos \theta_p)^{1/2}$. On the other hand, $\hat{\mathbf{s}}_*$ also precesses around \mathbf{J} , but at a much slower rate:

$$\frac{d\hat{\mathbf{s}}_*}{dt} \simeq (\omega_{*1} \cos^2 \theta_{1J} + \omega_{*p} \cos^2 \theta_{pJ}) (\cos \theta_{*J}) \hat{\mathbf{s}}_* \times \hat{\mathbf{J}}, \quad (11)$$

with a (approximately) constant θ_{*J} (the angle between $\hat{\mathbf{s}}_*$ and \mathbf{J}). (Of course, $\hat{\mathbf{s}}_*$ and \mathbf{J} mutually precess, conserving the total angular momentum.) Thus θ_{*1} varies between a minimum and maximum given by

$$(\theta_{*1})_{\min} \simeq |\theta_{*J} - \theta_{1J}|, \quad (12)$$

$$(\theta_{*1})_{\max} \simeq \theta_{*J} + \theta_{1J}. \quad (13)$$

For an initially aligned ($\theta_{*1} = 0$) system, we have

$$(\theta_{*1})_{\max} \simeq 2\theta_{1J} = 2 \sin^{-1} \left(\frac{L_p}{J} \sin \theta_p \right). \quad (14)$$

For $L_p \gg L_1$, this reduces to $(\theta_{*1})_{\max} = 2\theta_p$.

(ii) *Strong (planet-star) coupling regime* ($\epsilon_{*1} \ll 1$). In this regime, $\hat{\mathbf{s}}_*$ and $\hat{\mathbf{l}}_1$ precess around each other at a rapid rate, preserving the misalignment angle as an adiabatic invariant¹

$$\theta_{*1} \simeq \text{constant}. \quad (15)$$

The angle between \mathbf{L}_1 and $\mathbf{H} = \mathbf{S}_* + \mathbf{L}_1$ is also constant, and is given by $\sin \theta_{1H} = (S/H) \sin \theta_{*1}$. On the other hand, \mathbf{L}_p and \mathbf{H} mutually precess around each other at a slow rate, with a constant θ_{pH} (the angle between \mathbf{L}_p and \mathbf{H}). Thus, in the strong coupling regime, $\theta_{1p} = \theta_p$ is not constant, but varies between a minimum and maximum given by

$$(\theta_{1p})_{\min} \simeq |\theta_{pH} - \theta_{1H}|, \quad (16)$$

$$(\theta_{1p})_{\max} \simeq \theta_{pH} + \theta_{1H}. \quad (17)$$

For initially aligned systems ($\theta_{*1} = 0$), θ_p is approximately constant (since $\theta_{1H} = 0$). We can obtain the leading-order correction to the adiabatic result ($\theta_{*1} = 0$; see Eq. 15): the maximum and the RMS values of $|\sin \theta_{*1}|$ are given by (see Lai & Pu 2017)

$$|\sin \theta_{*1}|_{\max} \simeq \epsilon_{*1} |\sin 2\theta_p|, \quad (18)$$

$$\langle \sin^2 \theta_{*1} \rangle^{1/2} \simeq \frac{1}{\sqrt{2}} \epsilon_{*1} |\sin 2\theta_p|. \quad (19)$$

Note that these equations are valid for arbitrary values of θ_p .

(iii) *Resonance*. For $\epsilon_{*1} \sim 1$, resonant excitation of θ_{*1} becomes possible. More precisely, for small θ_{*1} and θ_p , resonance occurs when

$$\omega_{*1} + \omega_{*p} \simeq \omega_{1*} + \omega_{1p}, \quad (20)$$

which is equivalent to

$$\epsilon_{*1} \simeq \frac{1 - S_*/L_1}{1 + S_*/L_1}. \quad (21)$$

Obviously, since ω_{1p} is always larger than ω_{*p} , resonance is possible only when $S_* \lesssim L_1$. Finite θ_p tends to broaden or smooth out the resonance, although a significant ‘‘discontinuity’’ in the $(\theta_{*1})_{\max} - \epsilon_{*1}$ curve is still visible for $L_1/S_* \gtrsim$ a few [Fig. 1. See Appendix A of Lai & Pu (2017) for more details on the theory of resonance].

The above results/discussions are valid for arbitrary θ_p .

¹ This result was first derived by Goldreich (1965) for $S_* \gg L_1$ (in the context of planetary satellites, with the Sun acting as a perturber). The generalization to comparable S_* and L_1 is straightforward: Both \mathbf{S}_* and \mathbf{L}_1 precess rapidly around \mathbf{H} , while \mathbf{H} precesses around \mathbf{L}_p slowly; thus $\cos \theta_{*H}$ is adiabatically invariant because it is the ‘‘action’’ of a action-angle pair.

For $\theta_p \ll 1$, an analytical expression of $(\theta_{*1})_{\max}$ covering all three regimes can be obtained (Pu & Lai 2017).

3 HOT JUPITER SYSTEMS WITH EXTERNAL COMPANION

For a HJ around a solar-type star ($M_* \sim M_\odot$, $R_* \sim R_\odot$) with a giant planet ($m_p \sim M_J$) perturber at $\tilde{a}_p \sim 1$ au, we have

$$\omega_{*1} \simeq 4.8 \times 10^{-6} \left(\frac{6k_{q*}}{k_*} \right) \frac{m_1}{M_J} \left(\frac{a_1}{0.04 \text{ au}} \right)^{-3} \left(\frac{M_*}{M_\odot} \right)^{-1} \times \left(\frac{R_*}{R_\odot} \right)^3 \left(\frac{P_*}{30 \text{ d}} \right)^{-1} \frac{2\pi}{\text{yrs}}, \quad (22)$$

$$\omega_{1p} \simeq 6 \times 10^{-6} \frac{m_p}{M_J} \left(\frac{M_*}{M_\odot} \right)^{-1/2} \left(\frac{a_1}{0.04 \text{ au}} \right)^{3/2} \times \left(\frac{\tilde{a}_p}{1 \text{ au}} \right)^{-3} \frac{2\pi}{\text{yrs}}, \quad (23)$$

where $6k_{q*}/k_* \simeq 1$. Thus

$$\epsilon_{*1} = \frac{\omega_{1p}}{\omega_{*1}} \left(\frac{1 - \omega_{*p}/\omega_{1p}}{1 + S_*/L_1} \right) \simeq 1.25 \left(\frac{6k_{q*}}{k_*} \right)^{-1} \frac{m_p}{m_1} \left(\frac{a_1}{0.04 \text{ au}} \right)^{9/2} \left(\frac{\tilde{a}_p}{1 \text{ au}} \right)^{-3} \left(\frac{P_*}{30 \text{ d}} \right) \times \left(\frac{M_*}{M_\odot} \right)^{1/2} \left(\frac{R_*}{R_\odot} \right)^{-3} \left(\frac{1}{1 + S_*/L_1} \right), \quad (24)$$

where in the second equality we have used $\omega_{*p}/\omega_{1p} \ll 1$, and the angular momentum ratio is

$$\frac{S_*}{L_1} = 0.079 \left(\frac{k_*}{0.06} \right) \left(\frac{m_1}{M_J} \right)^{-1} \left(\frac{a_1}{0.04 \text{ au}} \right)^{-1/2} \left(\frac{P_*}{30 \text{ d}} \right)^{-1} \times \left(\frac{M_*}{M_\odot} \right)^{1/2} \left(\frac{R_*}{R_\odot} \right)^2. \quad (25)$$

3.1 Constrain External Perturbers of HJs Using Stellar Obliquities

Radial velocity detections of external companions of HJs give $m_p \sin i$ and a_p , e_p , but do not constrain θ_p . Rossiter-McLaughlin measurements yield the projected stellar obliquity λ , which is related to the 3D stellar obliquity θ_{*1} by

$$\sin^2 \theta_{*1} = \frac{\sin^2 \lambda}{1 - \cos^2 \lambda \cos^2 \phi}, \quad (26)$$

where ϕ is defined by $\hat{\mathbf{s}}_* = \sin \theta_{*1} (\hat{\mathbf{x}} \cos \phi + \hat{\mathbf{y}} \sin \phi) + \hat{\mathbf{l}}_1 \cos \theta_{*1}$, with $\hat{\mathbf{x}}$ along the line of sight. Several systems containing a HJ and external companion were recently considered by Becker et al. (2017) in an attempt to constrain θ_p , but they neglected the stellar spin-orbit coupling in their analysis.

In the following, we do not attempt to carry out full-blown statistical analysis. Instead, for each system, we evaluate the coupling parameter ϵ_{*1} , which immediately informs us whether the observed stellar obliquity is ‘‘permanent’’ or can vary due to an inclined perturber. In addition, assuming an initial $\theta_{*1} = 0$, we calculate the fraction of time f that the system spends with θ_{*1} less than certain value (as

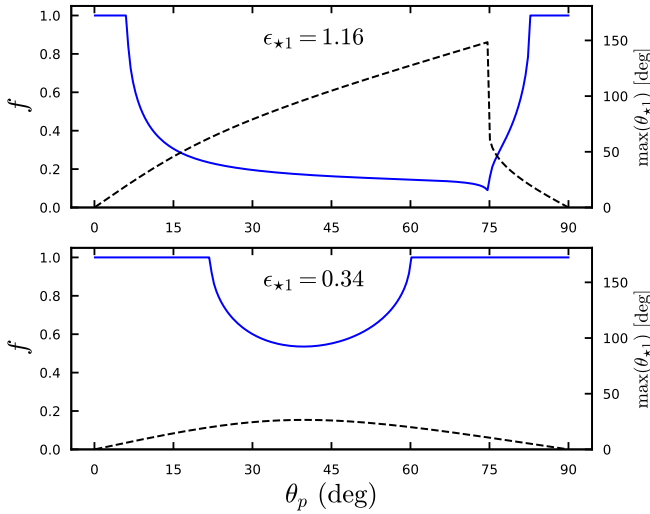


Figure 2. A typical HJ system with $m_1 = 1M_J$, $a_1 = 0.04$ au, orbiting a star with $M_* = 1M_\odot$, $R_* = 1R_\odot$, $P_* = 30$ days. An external companion has $m_p = 1M_J$, $a_p = 1$ au (top panel), and $a_p = 1.5$ au (bottom panel), leading to differing values of ϵ_{*1} , as labeled. Considering a low-obliquity HJ with projected obliquity λ constrained to be in the range $0 - 20^\circ$, we calculate the fraction of time f that θ_{*1} is within that range as a function of θ_p . The dashed lines depict the maximum value of θ_{*1} achieved over the integration timespan (1 Gyr). Note that in the upper panel, the maximum θ_{*1} for large θ_p is not equal to the theoretical $(\theta_{*1})_{\max}$ discussed in Section 2 (see Fig. 1); this is because for large θ_p , the precession time of \hat{l}_1 around \hat{l}_p can be longer than the integration time, so the system does not have time to reach the theoretical maximum θ_{*1} .

constrained by observations) for a range of θ_p 's. This would then provide an approximate constraint on θ_p .

Figure 2 illustrates our procedure. It highlights the importance of including spin-orbit coupling in the analysis and the role of the coupling parameter ϵ_{*1} . In particular, for $\epsilon_{*1} \lesssim 0.4$, even a highly inclined perturber would satisfy the observational constraint of small λ .

3.2 Specific Systems

3.2.1 HAT-P-13

This system ($M_* = 1.22^{+0.05}_{-0.10}M_\odot$, $R_* = 1.56 \pm 0.08R_\odot$) contains a HJ with $m_1 = 0.851 \pm 0.038M_J$, $a_1 = 0.0427^{+0.0006}_{-0.0012}$ au, and an external perturber with $m_p \sin i = 14.28 \pm 0.28M_J$, $a_p = 1.226$ au, $e_p = 0.6616 \pm 0.0054$ (Bakos et al. 2009; Winn et al. 2010). The star has a measured $v \sin i_* = 1.66 \pm 0.37$ km/s, yielding a stellar rotation period $P_* \simeq 47.5 \sin i_*$ days. The projected spin-orbit misalignment angle is $\lambda = 1.9^\circ \pm 8.5^\circ$. For concreteness, we adopt the measured mean values for various quantities and assume $\sin i = \sin i_* = 1$ (these loose assumptions will also be used for the other systems considered below). We then find $\epsilon_{*1} \simeq 14$. (Note that a larger m_p would increase ϵ_{*1} , while a smaller P_* would decrease ϵ_{*1} .) The system is therefore safely in the weak-coupling regime, and may have its

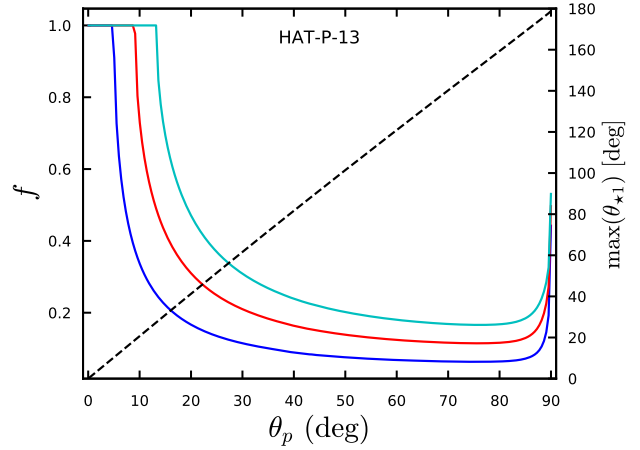


Figure 3. Similar to Fig. 2 but showing results for HAT-P-13. Fraction of time f with θ_{*1} spent in the observed range of obliquity, as a function of θ_p . We use the projected obliquity λ as an indicator of the range of true obliquity (which is generally larger than λ ; see Eq. 26). Blue (lower solid curve): θ_{*1} within 1σ of the observed λ ; red (middle solid curve): 2σ ; cyan (upper curve): 3σ . Dashed line: maximum value of θ_{*1} achieved over the integration timespan of 1 Gyr.

spin-orbit alignment disrupted if the perturber is sufficiently inclined (see Fig. 3).

3.2.2 WASP-41

This system ($M_* = 0.93 \pm 0.07M_\odot$, $R_* = 0.87 \pm 0.03R_\odot$) contains a HJ with $m_1 = 0.94 \pm 0.05M_J$, $a_1 = 0.040 \pm 0.001$ au, and an external perturber with $m_p \sin i = 3.18 \pm 0.2M_J$, $a_p = 1.07 \pm 0.03$ au, $e_p = 0.294 \pm 0.024$ (Neveu-VanMalle et al. 2016). RM measurement gives $\lambda = 6^\circ \pm 11^\circ$. The star has $v \sin i_* = 2.64 \pm 0.25$ km/s, yielding $P_* \simeq 16.7 \sin i_*$ days. Adopting the measured mean values for various quantities and assuming $\sin i = \sin i_* = 1$, we find $\epsilon_{*1} \simeq 2.9$. This system is in the weak coupling regime. The θ_p constraint is similar to that for HAT-P-13 (see Fig. 4).

3.2.3 WASP-47

This system ($M_* = 1.026 \pm 0.076M_\odot$, $R_* = 1.15 \pm 0.04R_\odot$) contains a HJ with $m_1 = 1.13 \pm 0.06M_J$, $a_1 = 0.051 \pm 0.001$ au, and an external perturber with $m_p \sin i = 1.24 \pm 0.22M_J$, $a_p = 1.36 \pm 0.04$ au, $e_p = 0.13 \pm 0.1$ (Neveu-VanMalle et al. 2016). The HJ also has two close low-mass neighbors (Becker et al. 2015), whose dynamical effects are negligible for this analysis. RM measurement gives $\lambda = 0 \pm 24^\circ$ (Sanchis-Ojeda et al. 2015). The star has $v \sin i_* = 1.3 \pm 1$ km/s (Sanchis-Ojeda et al. 2015) or 3.0 ± 0.6 km/s (Hellier et al. 2012). Choosing $v \sin i_* = 1.3$ km/s yields $P_* \simeq 44.8 \sin i_*$ days. As a result, $\epsilon_{*1} \simeq 1.6$, putting the system in the weak coupling regime. Note that ϵ_{*1} can be easily smaller by a factor of two or more, given the uncertainty in P_* . Overall, because of the large error in the λ measurement, θ_p is not well constrained (see Fig. 5).

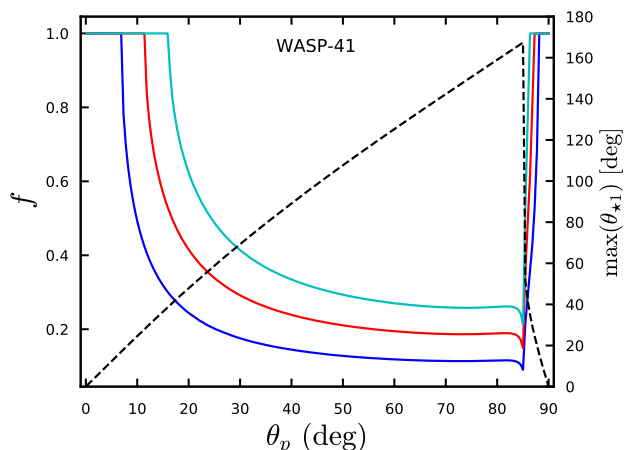


Figure 4. Same as Fig. 3 but showing results for WASP-41.

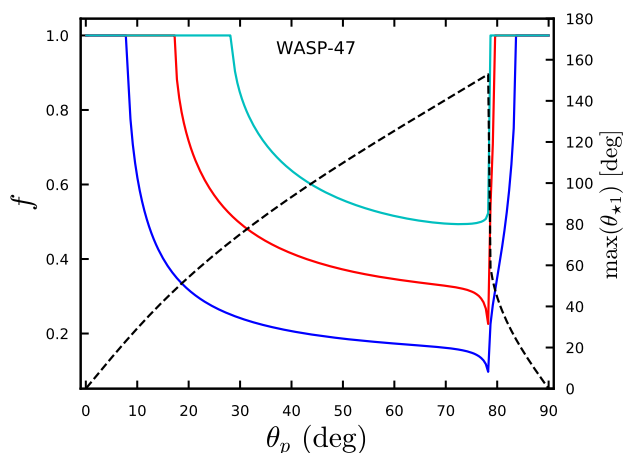


Figure 5. Same as Fig. 3 but showing results for WASP-47.

3.2.4 WASP-22

This system ($M_* = 1.109 \pm 0.026 M_\odot$, $R_* = 1.219^{+0.052}_{-0.033} R_\odot$) contains a HJ with $m_1 = 0.588 \pm 0.017 M_J$, $a_1 = 0.04698 \pm 0.00037$ au, and observed linear RV trend of ~ 40 m/s/yr, indicating the presence of an external perturber (Maxted et al. 2010; Anderson et al. 2011). The projected mass and semi-major axis of the perturber are constrained in the combination $m_p \sin i/a_p^2$ (see Fig. 10 of Knutson et al. 2014). RM measurement gives $\lambda = 22^\circ \pm 16^\circ$. For a planetary or brown dwarf ($m_p \lesssim 30 M_J$) companion, this system is always in the strong-coupling regime with $\epsilon_{*1} \ll 1$, so that the perturber is unable to change the spin-orbit angle from the initial value for any value of θ_p . Whatever the observed value θ_{*1} must be “permanent”, and no meaningful constraint on θ_p can be obtained (see the lower panel of Fig. 2).

4 SPIN-ORBIT MISALIGNMENT IN MULTI-PLANET SYSTEMS: KEPLER-56

Our analysis can be generalized to multi-planet systems with spin-orbit misalignment measurements. Here we use Kepler-56 as an example to illustrate our method, as this is the only such system with significant stellar obliquity (Huber et al. 2013).

Kepler-56 (with a red giant host star $M_* = 1.32 M_\odot$, $R_* = 4.23 R_\odot$, $P_* = 74$ days) has two transiting planets ($m_{1,2} = 0.0925, 0.60 M_J$) at $a_{1,2} = 0.103, 0.165$ au (period 10.5, 21 days). The orbits of the two planets are coplanar within $\sim R_*/a_2 = 6.8^\circ$, and are inclined with respect to the stellar equator by more than 37° (Huber et al. 2013). An external perturber has been found through RV observations, with $a_p = 2.15$ au, $e_p = 0.2$, and $m_p \sin i \simeq 5.6 M_J$ (Otor et al. 2016).

The mutual coupling between the two inner planets against the forcing from the perturber can be measured by the parameter (Lai & Pu 2017)

$$\epsilon_{12} \equiv \frac{\omega_{2p} - \omega_{1p}}{\omega_{12} + \omega_{21}}, \quad (27)$$

where the ω 's have the similar meanings as in Section 2. We find $\epsilon_{12} \simeq 2.3 \times 10^{-3} / \sin i$, implying that the inner two planets are strongly coupled and their coplanarity is not affected by any external perturbers that satisfy the current RV constraint (regardless of θ_p). It is also easy to check that the two planets are strongly coupled with respect to the perturbation from the stellar quadrupole.

Thus, the two inner planets tend to precess around \hat{l}_p as a “rigid” body, with characteristic frequency

$$\omega_{12,p} = \frac{L_1 \omega_{1p} + L_2 \omega_{2p}}{L_1 + L_2} \simeq \frac{2\pi}{4.3 \times 10^4 \text{ yrs}} \left(\frac{m_p}{5.6 M_J} \right). \quad (28)$$

The two inner planets also drive the star into precession, with characteristic frequency

$$\omega_{*,12} = \omega_{*1} + \omega_{*2} \simeq \frac{2\pi}{6.7 \times 10^5 \text{ yrs}} \left(\frac{6k_{q*}}{k_*} \right). \quad (29)$$

The precession of $\hat{l}_1 \simeq \hat{l}_2$ around \hat{s}_* is

$$\omega_{12,*} = \left(\frac{S_*}{L_1 + L_2} \right) \omega_{*,12} \simeq 0.49 \left(\frac{k_*}{0.06} \right) \omega_{*,12}. \quad (30)$$

Thus the coupling parameter between \hat{s}_* and $\hat{l}_{1,2}$ relative to the forcing from m_p is

$$\epsilon_{*,12} = \frac{\omega_{12,p} - \omega_{*,p}}{\omega_{*,12} + \omega_{12,*}} \simeq 15.6 \left(\frac{m_p}{5.6 M_J} \right) \frac{k_*/(6k_{q*})}{1 + 8k_*}. \quad (31)$$

Even with the uncertainties of various parameters, the inner two planets are weakly coupled to the stellar spin. The stellar obliquity (relative to $\hat{l}_{1,2}$) therefore varies between $|\theta_{*p} - \theta_{12,p}|$ and $\theta_{*p} + \theta_{12,p}$ (see Eqs. 12-13; note that since $L_p \gg L_{12} = L_1 + L_2$ for this system, \hat{J} is aligned with \hat{l}_p). The observed stellar obliquity ($\lambda \geq 37^\circ$) then implies $\theta_{*p} + \theta_{12,p} \geq 37^\circ$ (see Li et al. 2014 for a previous analysis).

5 DISCUSSION

A main goal of this paper is to inform the readers that there is a simple way to assess the dynamical role of external perturbers on the spin-orbit misalignments of planetary sys-

tems. The key is to evaluate the star-planet spin-orbit coupling parameter (Eq. 9) in response to the differential precession induced by the external companion. We have presented analytic results in various limiting regimes, and discussed how the general results (see Fig. 1) scale with different physical parameters (Section 2). Similar analysis can be done for multi-planet systems (Section 4), with the generalized spin-orbit coupling parameter given by Eq. (31).

As alluded to in Section 1, continuing observations on spin-orbit misalignments and external companions in hot Jupiter (HJ) and other compact planetary systems may shed light on the formation mechanism of close-in planets. Several recent works of such systems have either neglected some key physical ingredients (spin-orbit coupling) or made such a relatively simple problem unnecessarily complex or obscure. We hope that the results of this paper (see also Lai 2016) will make future analysis simpler and more transparent.

A recent analysis on spin-orbit alignments of HJs around cool stars concluded that the exterior companions are coplanar (Becker et al. 2017). While this may be the case of a few systems with gas giant companion at ~ 1 au, similar conclusions cannot be drawn for systems with a slightly more distant companion (see Section 3, especially Fig. 2) since the spin-orbit coupling parameter ϵ_{*1} depends sensitively on the perturber's semi-major axis ($\epsilon_{*1} \propto a_p^{-3}$; see Eq. 24).

Certain HJ formation mechanisms (e.g. Lidov-Kozai migration) require an external companion with a high inclination ($> 40^\circ$). As a result, constraints placed on the mutual inclination via the method discussed in this paper may in principle lead to a constraint on the migration mechanism. However, we emphasize that the inclination of giant planet companion may only be constrained when it is relatively close (at 1 au, so that $\epsilon_{*1} \gtrsim 1$, see Eq. 24), such as for WASP-41 and HAT-P-13. These systems clearly could not have formed in the classic LK migration picture (with the HJ originating at 1 au or beyond), because the initial configuration would be unstable. Lidov-Kozai migration requires a much more distant companion (at, say 5-10 au, so that the initial configuration is stable). Such a companion will satisfy $\epsilon_{*1} \ll 1$, so that it is unable to affect the star-HJ misalignment, and therefore no constraint on the mutual inclination may be inferred. We conclude that in practice, using low stellar obliquities to constrain mutual inclinations is unlikely to be useful in identifying/ruling out whether Lidov-Kozai migration occurred in HJ systems.

ACKNOWLEDGMENTS

This work has been supported in part by NASA grants NNX14AG94G and NNX14AP31G, and NSF grant AST-1715246. KRA is supported by a NSF graduate fellowship and BP by a NASA graduate fellowship (NESSF).

REFERENCES

Anderson, D. R., Collier Cameron, A., Gillon, M., et al. 2011, *A & A*, 534, A16
 Anderson, K.R., Storch, N.I., Lai, D. 2016, *MNRAS*, 456, 3671

Antonini, F., Hamers, A.S., Lithwick, Y. 2016, *ApJ*, submitted (arXiv:1604.01781)
 Bakos, G. Á., Howard, A. W., Noyes, R. W., et al. 2009, *ApJ*, 707, 446
 Bate, M.R., Lodato G. & Pringle J.E., 2010, *MNRAS*, 401, 1505
 Batygin, K. 2012, *Nature*, 491, 418
 Batygin, K., & Adams, F. C. 2013, *ApJ*, 778, 169
 Beauge, C., Nesvorný, D. 2012, *ApJ*, 751, 119
 Becker, J. C., Vanderburg, A., Adams, F. C., Rappaport, S. A., & Schwengeler, H. M. 2015, *ApJL*, 812, L18
 Becker, J. C., Vanderburg, A., Adams, F. C., Khain, T., & Bryan, M. 2017, arXiv:1710.01737
 Boue, G., Fabrycky, D.C. 2014, *ApJ*, 789, 110
 Bryan, M., et al. 2016, *ApJ*, 821, 89
 Fabrycky, D., & Tremaine, S. 2007, *ApJ*, 669, 1298
 Goldreich, P. 1965, *AJ*, 70, 5
 Hellier, C., Anderson, D. R., Collier Cameron, A., et al. 2012, *MNRAS*, 426, 739
 Huber, D., et al. 2013, *Science*, 342, 331
 Knutson, H. A., Fulton, B. J., Montet, B. T., et al. 2014, *ApJ*, 785, 126
 Lai, D. 2014, *MNRAS*, 440, 3532
 Lai, D. 2016, *AJ*, 152, 215
 Lai, D., Foucart, F., & Lin, D. N. C. 2011, *MNRAS*, 412, 2790
 Lai, D., Pu, B. 2017, *AJ*, 153, 42
 Li, G., et al. *ApJ*, 794, 131
 Liu, B., Munoz, D.J., Lai, D. 2015, *MNRAS*, 447, 747
 Maxted, P. F. L., Anderson, D. R., Gillon, M., et al. 2010, *AJ*, 140, 2007
 Mecheri, R., Abdelatif, T., Irbah, A., Provost, J., Berthomieu, G. 2004, *Solar Phys.*, 222, 191
 Munoz, D.J., Lai, D., Liu, B. 2016, *MNRAS*, 460, 1086
 Nagasawa, M., Ida, S., & Bessho, T. 2008, *ApJ*, 678, 498
 Naoz, S., Farr, W. M., & Rasio, F. A. 2012, *ApJ*, 754, LL36
 Neveu-VanMalle, M., Queloz, D., Anderson, D. R., et al. 2016, *A & A*, 586, A93
 Ngo, H., Knutson, H. A., Hinkley, S., et al. 2015, *ApJ*, 800, 138
 Ngo, H., Knutson, H. A., Hinkley, S., et al. 2016, *ApJ*, 827, 8
 Otor, O.J., et al. 2016, *AJ*, 152, 165
 Petrovich, C. 2015, *ApJ*, 799, 27
 Pu, B., Lai, D. 2017, *MNRAS*, submitted
 Sanchis-Ojeda, R., Winn, J. N., Dai, F., et al. 2015, *ApJL*, 812, L11
 Spalding, C., Batygin, K. 2014, *ApJ*, 790, 42
 Storch, N. I., Anderson, K. R., & Lai, D. 2014, *Science*, 345, 1317
 Wang, J., Fischer, D. A., Horch, E. P., & Xie, J.-W. 2015, *ApJ*, 806, 248
 Winn, J. N., & Fabrycky, D. C. 2015 *ARAA*, 53, 409
 Winn, J. N., Johnson, J. A., Howard, A. W., et al. 2010, *ApJ*, 718, 575
 Wu, Y., Murray, N.W., & Ramshhai, J.M. 2007, *ApJ*, 670, 820
 Wu, Y., & Lithwick, Y. 2011, *ApJ*, 735, 109